Mechanisms of Epithelial Cell–Cell Adhesion and Cell Compaction Revealed by High-resolution Tracking of E-Cadherin–Green Fluorescent Protein

Cynthia L. Adams, Yih-Tai Chen, Stephen J Smith, and W. James Nelson

Department of Molecular and Cellular Physiology, Stanford University School of Medicine, Stanford, California 94305-5345

Abstract. Cadherin-mediated adhesion initiates cell reorganization into tissues, but the mechanisms and dynamics of such adhesion are poorly understood. Using time-lapse imaging and photobleach recovery analyses of a fully functional E-cadherin/GFP fusion protein, we define three sequential stages in cell–cell adhesion and provide evidence for mechanisms involving E-cadherin and the actin cytoskeleton in transitions between these stages. In the first stage, membrane contacts between two cells initiate coalescence of a highly mobile, diffuse pool of cell surface E-cadherin into immobile punctate aggregates along contacting membranes. These E-cadherin aggregates are spatially coincident with membrane attachment sites for actin filaments branching off from circumferential actin cables that circumscribe each cell. In the second stage, circumferential actin cables near cell–cell contact sites separate, and the resulting two ends of the cable swing outwards to the perimeter of the contact. Concomitantly, subsets of E-cadherin puncta are also swept to the margins of the contact where they coalesce into large E-cadherin plaques. This reorganization results in the formation of a circumferential actin cable that circumscribes both cells, and is embedded into each E-cadherin plaque at the contact margin. At this stage, the two cells achieve maximum contact, a process referred to as compaction. These changes in E-cadherin and actin distributions are repeated when additional single cells adhere to large groups of cells. The third stage of adhesion occurs as additional cells are added to groups of >3 cells; circumferential actin cables linked to E-cadherin plaques on adjacent cells appear to constrict in a purse-string action, resulting in the further coalescence of individual plaques into the vertices of multicell contacts. The reorganization of E-cadherin and actin results in the condensation of cells into colonies. We propose a model to explain how, through strengthening and compaction, E-cadherin and actin cables coordinate to remodel initial cell–cell contacts to the final condensation of cells into colonies.

Key words: cadherin • actin • cell–cell adhesion • epithelia • microscopy

Cell–cell adhesion is crucial for the development and survival of multicellular organisms (Townes and Holtfreter, 1955; Takeichi, 1991; Steinberg, 1996). Members of the cadherin superfamily of Ca^{2+}-dependent cell–cell adhesion proteins are expressed in most organs and tissues of vertebrates and invertebrates. Different cadherins are expressed in specific tissues, cell layers, and neuronal cell types consistent with their roles in distinct cellular recognition and sorting processes (Takeichi, 1987; Nose et al., 1988; Takeichi, 1991; Steinberg and Takeichi, 1994; Fannon and Colman, 1996; Uchida et al., 1996; Martinek and Gaul, 1997). While recent studies have attempted to elucidate the molecular and mechanical properties of cadherin-mediated adhesion (Brieher et al. 1996; Yap et al., 1997), little is known about the physical or molecular dynamics of cell–cell adhesion (cell stickiness), compaction (maximization of adhesive contacts), or condensation (aggregation of large cell colonies) during tissue formation.

Cadherins are single transmembrane–spanning proteins. The extracellular domain (amino terminus) is composed of five repeats that have similar structures and contain Ca^{2+}-binding motifs (Shapiro et al., 1995; Aberle et al., 1996). While homotypic binding between the extracellular domains of cadherins on adjacent cells is clearly important for cell–cell recognition (Nose et al., 1988), the affinity of

The current address of Cynthia L. Adams is Cytokinetics, Inc., 280 East Grand Ave., South San Francisco, CA 94040.

Address all correspondence to Stephen J Smith, Department of Molecular and Cellular Physiology, Beckman Center, Stanford University School of Medicine, Stanford, CA 94305-5345. Tel.: 650-723-6799; Fax: 650-498-5286; E-mail: sjsmith@leland.stanford.edu

binding (~1 μM; Shapiro et al., 1995) may not be sufficient to promote the strong cell–cell adhesion necessary to maintain tissue integrity. X-ray diffraction studies of crystals of the amino-terminal repeat domains of E-cadherin and N-cadherin revealed the presence of dimers and higher ordered complexes (Nagar et al., 1996; Shapiro et al., 1995). Formation of higher-order complexes between extracellular domains of parallel-oriented cadherins on single cells and clustering of extracellular E-cadherin between cells might cooperatively increase the strength of adhesion (Brieher et al., 1996; Yap et al., 1997), but little is known about how, when, or where clustering of cadherins occurs during cell–cell adhesion in vivo.

The cytoplasmic domain of cadherin is also required for cell–cell adhesion. The amino acid sequences of the cytoplasmic domain of different cadherins are very similar, and contain a highly conserved binding site for a family of sequence-related cytosolic proteins: β-catenin, plakoglobin, and $p120^{CAS}$ (Aberle et al., 1994; Jou et al., 1995; Ozawa et al., 1989; Reynolds et al., 1994). The cadherin/β-catenin complex binds via β-catenin to another cytosolic protein, α-catenin (Herrenknecht et al., 1991; Jou et al., 1995; Ozawa and Kemler, 1992), which interacts with actin filaments either directly (Rimm et al., 1995) or through other actin-associated proteins such as α-actinin (Knudsen et al., 1995). Binding of this protein complex to the actin cytoskeleton is consistent with the appearance of a pool of cadherins and catenins at cell–cell contacts that is resistant to extraction by the nonionic detergent Triton X-100 (Nagafuchi and Takeichi, 1988; Ozawa et al., 1989).

In individual motile cells, actin filaments are continually polymerizing at the free cell edge of lamellae, and depolymerizing in a transition zone between the cell body and lamellae. This transition zone is often characterized by a conspicuous ring of actin that is called a circumferential actin cable (see review, Small et al., 1996). In single motile epithelial cells, such actin cables often circumscribe the cell in the form of a continuous ring. In polarized epithelial cells, actin filaments are also organized into a much thinner, much more peripherally disposed circumferential ring at the apical surface in association with the adherens junction (Hirano et al., 1987); this actin organization is also referred to as a circumferential actin cable. While circumferential actin structures are thus characteristic of both motile and tissue forms of epithelial cells, a dramatic structural transformation in actin organization occurs during the formation and stabilization of cell–cell contacts. Recent studies have suggested that circumferential actin cables in single cells either passively become parallel to cell–cell contacts (Yonemura et al., 1995) or they actively reorganize to the cell periphery (Gloushankova et al., 1997). These studies have not provided significant insight into how actin filaments in lamellae and circumferential actin cables reorganize when two lamellae interact in forming a cell–cell contact. Thus, while the actin cytoskeleton is known to be involved in cadherin-mediated cell–cell adhesion, little is known about how actin participates in the initiation and strengthening of cell–cell adhesion, or how the organization of the actin cytoskeleton in single motile cells becomes incorporated into the actin organization observed in monolayers of polarized epithelial cells.

Even less is known about the molecular mechanisms of compaction and condensation of single cells into multicellular colonies. On the other hand, much work has been done to elucidate the mechanisms involved in the healing of wounded monolayers and tissues (Martin and Lewis, 1992; Bement et al., 1993). Small wounds in cell monolayers rapidly form circumferential actin cables at the wound perimeter, which then slowly cinch together with a purse-string action (Bement et al., 1993; Brock et al., 1996). Similarly, tissue explants with ragged edges will round up in vitro over extended periods of time, presumably by a similar purse-string action. The mechanisms that mediate these events could play a role in the genesis of multicellular monolayers, but previous studies have not established similarities among these processes.

The experimental approaches used in the studies described above have not provided much insight into the dynamic processes by which cadherins, catenins, and the actin cytoskeleton cooperate to initiate, strengthen, and compact cell–cell contacts between cells initiating adhesion or reorganizing within colonies. In previous studies, we used differential interference contrast (DIC) time-lapse imaging coupled with retrospective immunocytochemistry to examine the distributions of E-cadherin, catenins, and actin in adhering MDCK cells (McNeill et al., 1993; Adams et al., 1996). We showed that during the first hour of cell–cell adhesion, E-cadherin, β-catenin, and α-catenin coaccumulated into Triton X-100–insoluble aggregates (puncta) that are associated with thin actin bundles (Adams et al., 1996). However, from these previous studies many problems related to initiation of cell–cell adhesion were unresolved. For example, we were unable to determine the relationship of Triton X-100 insolubility and clustering of E-cadherin, the source of E-cadherin in puncta, the role of the actin cytoskeleton in the spatial organization of puncta, the dynamics and fate of puncta within the contact, or the dynamics of actin and cadherin reorganization in older contacts. Furthermore, we were unable to investigate the role(s) of these E-cadherin puncta in strengthening and compacting initial adhesive contacts, or the mechanisms of reorganization of cell–cell contacts as cells condensed into colonies to form a multicell monolayer. Answers to these problems are at the core of understanding mechanisms involved in cell–cell adhesion.

In the present study, we examined the dynamics of cell–cell adhesion using a fully functional protein comprising E-cadherin fused to green fluorescent protein (EcadGFP).[1] EcadGFP was stably expressed in MDCK epithelial cells, and was examined with time-lapse imaging and photobleach-recovery analysis. We define three sequential stages in cell–cell adhesion, and show how the distributions of E-cadherin and the actin cytoskeleton are remodeled to coordinate transitions in cell–cell adhesion from initial contacts, to strengthening and compaction, to the final condensation of cells into colonies. Our results provide new detailed insights into the dynamics and mechanisms involved in regulating epithelial cell–cell adhesion in vivo.

1. *Abbreviations used in this paper*: CD, cytochalasin D; DIC, differential interference contrast; EcadGFP, E-cadherin fused to green fluorescent protein; synGFP, synthetic jellyfish green fluorescence protein; TIP, time, intensity, and position.

Materials and Methods

Construction of E-cadherin–GFP Recombinant cDNA and Stable Transfection of MDCK Cells

Recombinant cDNA of a synthetic jellyfish green fluorescence protein (synGFP; Haas et al., 1996; a gift from Dr. Brian Seed) was used as the PCR template to amplify the complete synGFP coding region, with Xho1 and Not1 sites added to the 5′ and 3′ ends, respectively. The PCR product was subcloned into CDM8FluTag (Chen et al., 1993) through Xho1/Not1 sites that generated the plasmid HA-synGFP. A second PCR reaction using canine E-cadherin cDNA as the template amplified the complete coding region of E-cadherin (without a stop codon) with a Hind3 site added at the 5′ end and a Xho1 site added at the 3′ end. The PCR product was subcloned into HA-synGFP through Hind3 and Xho1 sites after restriction of HA-synGFP with Hind3 and Xho1 to release the influenza virus hemagglutin tag (Chen et al., 1993), and resulted in an in-frame fusion of E-cadherin and synGFP with the Xho1 site as the linker (U-GFP1). Most of the extracellular domain of E-cadherin–GFP fusion protein cDNA was then replaced with a Hind3/Bgl2 fragment from the cDNA of E-cadherin pCEcad1 after restricting U-GFP1 with Hind3/Bgl2 enzymes, to generate U-GFP2. Accordingly, there is no sequence difference between the coding regions for E-cadherin–GFP fusion protein in U-GFP1 and U-GFP2, but most of the extracellular domain encoded by U-GFP2 is from the E-cadherin cDNA instead of the PCR product. The E-cadherin-GFP fusion cDNA in U-GFP2 was confirmed by restriction mapping and DNA sequencing, and was used for transfection. MDCK IIG cells were transfected with U-GFP2 using Ca^{2+} phosphate (Graeve et al., 1990) with pSV2neo (Southern et al., 1982) as the selection marker. Eight positive clones expressing the E-cadherin–GFP fusion cDNA in U-GFP2 (EcadGFP) were isolated using cloning rings, and all clones gave identical patterns of EcadGFP fluorescence and Western blot profiles.

Expression of EcadGFP in Mouse L-Cells

To express EcadGFP in Ltk-cells stably, the E-cad-GFP cDNA was released from pUGFP2 by Hind3 and Not1 digestion, and was subcloned into the retroviral vector LZRS-pBMN-Z (Kinsella and Nolan, 1996) after restriction by Hind3 and Not1. Production of virus and infection of Ltk− cells was performed as previously reported (Kinsella and Nolan, 1996).

Cell-Cell Adhesion Mediated by EcadGFP

Aggregation. Ltk-cells and Ltk-cells stably transfected with U-GFP1 were tested for their ability to aggregate in suspension culture. Approximately 0.5×10^6 single cells were plated in DMEM containing 5 μM Ca^{2+} and 10% FCS that had been dialyzed extensively against PBS, or normal DMEM/FBS (1.8 mM Ca^{2+}) on 35-mm tissue culture dishes coated with 2% agarose (Sigma Chemical Co., St. Louis, MO) and left in a tissue culture incubator overnight. The organization of cells in clumps were recorded 18 h after plating using a Zeiss Axiovert microscope equipped with a 10× phase-contrast objective.

Kinetics of aggregation. Wild-type MDCK type G cells, MDCK cells expressing EcadGFP, and MDCK cells expressing EcadGFP treated for 24 h with 5 mM sodium butyrate were suspended with trypsin/EGTA treatment, counted, and adjusted to a density of 7×10^6 cells/ml in imaging buffer (DMEM without phenol red, 10% FBS, 50 mM Hepes). Cells were allowed to recover for 2 h before aggregation measurements. Cells were vortexed for 30 s immediately before loading into the cuvette of the aggregometer. Cells were immediately placed in an optical aggregometer (Model 440; Chrono-log, Corp., Havertown, PA) at 37°C. 270 μl of cells were transferred to a 0.6-mm diameter cuvette, and were kept in suspension by constant stirring at 300 rpm. Spontaneous aggregation was measured by monitoring the increase in OD of the cell suspension on a strip-chart recorder for up to 6 h with cell-free buffer as a reference. Maximal aggregation was determined by the value when changes in the transmitted light were zero. The half-time was manually determined as the time at half-maximal aggregation.

Binding of Catenins to EcadGFP in HEK 293 Cells and MDCK Cells

HEK 293-EBNA cells (Invitrogen Corp., Carlsbad, CA) were transfected with the E-cadherin-GFP plasmid, U-GFP2, using lipofectamine (GIBCO BRL, Gaithersburg, MD). 24 h after transfection, cells in one 35-mm dish were labeled with 250 μCi of [^{35}S]Met/Cys (Amersham Life Science, Inc., Arlington Heights, IL) for 24 h. At the end of the labeling period (48 h after transfection), cells were lysed in Triton X-100 lysis buffer (10 mM Tris-HCl, pH 7.5, 120 mM NaCl, 25 mM KCl, 2 mM EDTA, 2 mM EGTA, 0.5% Triton X-100), and proteins were immunoprecipitated with mAb 3G8, which binds to the extracellular domain of E-cadherin. The immunoprecipitate was resolved by 7.5% SDS-PAGE, and the radioactive signals were detected by fluorography. Identical labeling and immunoprecipitation experiments were performed with MDCK IIG cells stably transfected with U-GFP2.

Delivery of EcadGFP to the Basal-lateral Membrane of Polarized MDCK Cells

Confluent monolayers of MDCK cells stably transfected with U-GFP2 were grown on Transwell™ filters (Costar Corp., Cambridge, MA) for 7 d, and were treated with 5 mM sodium butyrate for 24 h before an experiment. Cells were first incubated with Met/Cys-free medium for 45 min, and then cells on one 24-mm diameter petri dish were labeled with 250 μCi of [^{35}S]Met/Cys for 1 h. After labeling, plasma membrane domain–specific biotinylation was performed as previously described (Wollner et al., 1992). Cells were lysed in Triton X-100 extraction buffer, and proteins in the lysate were immunoprecipitated with mAb 3G8. Biotinylated protein from the immunoprecipitates was collected with immobilized avidin (Pierce, Rockford, IL). Precipitated proteins were resolved by 7.5% SDS-PAGE. Radioactive signals were detected by fluorography.

Cell Culture

Stably transfected EcadGFP MDCK cells were maintained at low density in DMEM (Gibco Laboratories, Grand Island, NY) supplemented with 10% FBS (Summit, Ft. Collins, CO). 12–24 h before experimentation, 5 mM sodium butyrate in DMEM/FBS was added to 90% confluent cultures of cells to further induce expression of EcadGFP. Cells were removed with trypsin and plated at low density in DMEM/FBS on collagen-coated coverslips for 2–5 h. For time-lapse imaging, cells were removed from the incubator, and the media was replaced with imaging buffer (DME without phenol red, 10% FBS, 50 mM Hepes). The coverslip was placed in a custom-built imaging chamber with 500 μl of imaging buffer. Cytochalasin D (Sigma Chemical Co.) solution was diluted 1:2,000 from a stock solution in DMSO to 2 μM in the imaging buffer.

Time-lapse Imaging

The Smith Mark IV multisite laser scanning confocal microscope, designed by Stephen Smith and built by Stanford's Physiology Instrument Shop, has been described elsewhere (Adams et al., 1996). In brief, it is an optical bench design using argon (488 nm) and helium-neon (633 nm) lasers, a mirror galvanometer–based scanning unit, a GaAs photomultiplier and silicon photodiode photodetectors, and a PC-based control and data acquisition unit. It allows collection of multispectral fluorescence and transmitted light (e.g., Nomarski DIC) images in perfect spatial register as determined by a single laser scanning geometry. The multisite feature (see Cooper and Smith, 1992; McNeill et al., 1993; Adams et al., 1996; software written by Dr. Noam Ziv) provides for the acquisition of time-lapse sequences at multiple specimen areas by frequent automated motions of a motorized specimen stage combined with use of an autofocusing algorithm. For observing the maturation of cell–cell contacts, time-lapse sequences were collected at 6–12 stage-position sites with consecutive DIC and fluorescence images every 2–10 min for 2–23 h at 37°C. For tracking the dynamics of new puncta, images were collected at single sites every 0.9 s to 1 min for 3–100 min.

Image Analysis

To generate time, intensity, and position graphs (TIP scans), images were rotated in Adobe Photoshop (Adobe Systems, Inc., Mountain View, CA) so that the long axis of the contact in the last image of the time series was parallel to the horizon. The rotated images were imported into MetaMorph software (Universal Imaging Corp. West Chester, PA), and the developing contact area was boxed off by 50–200 adjacent horizontal regions, 2 pixels high by 60–200 pixels wide, depending on the relative position and length of the contact through the time sequence. MetaMorph software automatically collected maximum and integrated intensity data from contact, noncontact, and noncell (background) regions for all time

points. These data were then imported into Excel (Microsoft, Redmond, WA) and were corrected for photobleaching during the imaging period (<10%). Three-dimensional graphs were generated in Excel, and the pseudocolor intensity scale was created for ease of interpretation by color-blind persons and after photocopying (Livingstone, 1988). Intensity values from regions not in the contact were set to zero (black).

To determine the extent of clustering of existing vs. accumulation of new EcadGFP to the developing plaque area, measurements of the maximum fluorescence intensity and the sum of fluorescence intensities of all pixels in an area of fixed size were monitored. For analysis, time-lapse images were passed through a 3 × 3 convolution filter. A region of ~20 μm^2 was placed over an area where multiple small puncta were coalescing into a plaque at the edge of a developing cell–cell contact. The maximum and integrated intensities were measured using MetaMorph during the time-lapse series.

Photobleach Recovery

Method. Photobleaching experiments were performed on the scanning laser confocal microscope described above, and with EcadGFP cells prepared as for time-lapse experiments. The Smith Mark IV microscope incorporates a digitally controlled acousto-optic shutter (NEOS, Melbourne, FL). In conjunction with appropriate interface electronics and control software, this high-speed shutter allows the scanning laser beam to be turned on or off anywhere within the imaging area on a pixel-by-pixel basis. For the present experiments, the shutter was used for controlled photobleaching of circular areas within the scanning raster pattern. Typically, circular spots of a 120 pixel radius were generated with a 380 × 240 pixel scan raster. The actual spot radius at the specimen was varied by adjusting pixel sizes within the range of 0.01–0.05 μm. Scan geometries and beam intensities were varied independently as necessary during successive baseline acquisition, photobleaching, and recovery acquisition episodes. Scanning frame rates were varied to suit the needs of individual experiments between 0.33 and 3 Hz. Photobleaching energies were adjusted by varying exposure intensities and durations to achieve depths of photobleaching ranging from 30 to 70%. Calibrations of the exact position and dimensions of the photobleached area were collected using fixed specimens and aminopropysilane coverslips (Sigma Chemical Co.) coated with fluorescein-isothiocyanate (data not shown). The region of the cell to be photobleached was controlled by adjusting the x, y stage on the microscope during low-power imaging until the desired target area on the cell was in the middle of the video monitor.

Analysis. Digital images from the photobleaching experiments were imported into MetaMorph and passed through a 3 × 3 low-pass convolution filter. Average fluorescence intensity data from the bleached regions, two non-cell regions, and two non-bleached cell regions were collected for all frames. Data were imported into Excel and corrected for the minor photobleaching caused by the fluorescence recording process by normalization to a region outside the main photobleach pulse spot. The photobleaching recovery part of the data was then imported into Igor Pro, and the characteristic diffusion time (t_d) was calculated using equations for diffusion into a circular disk (Axelrod et al., 1976) and modified for total recovery (Soumpasis, 1983; equation 16). The diffusion coefficient (D) was calculated according to the equation

$$D = 0.224 * r^2 / t_d$$

where r is the radius of the bleached region. Mobile fraction constants were calculated according to equation in Axelrod (1976; equation 9) at indicated times after recovery. Measurements of the slower photobleach recovery timecourses were subject to potential errors due to gradual redistribution motions of puncta and plaques during recovery phases. TIP scans of photobleach recoveries were generated (see Fig. 9) and used to reject data from any experiment where such errors might have been significant.

Results

EcadGFP Binds Catenins, is Targeted to Cell–Cell Contact Sites, and has Adhesive Properties Identical to Those of E-cadherin

To examine directly the dynamics of E-cadherin in living cells, we constructed a fusion protein composed of full-length canine E-cadherin fused at the carboxyl terminus to GFP (EcadGFP). EcadGFP was expressed in MDCK cells (Fig. 1, *B* and *D*), HEK 293 EBNA cells (Fig. 1, *A* and *C*), and L cells (Fig. 1 *E*). In all cell types, EcadGFP had an apparent molecular mass of ~150 kD (Fig. 1, *A* and *B*) consistent with the combined molecular masses of the fused proteins; a minor protein band of ~160 kD was the likely precursor. Expression of endogenous E-cadherin in MDCK cells was suppressed to some extent in the presence of EcadGFP (Fig. 1 *B*); thus, EcadGFP contributes significantly to cell–cell adhesion in these MDCK cells. Analysis of EcadGFP-immunoprecipitated protein complexes showed the presence of three additional bands at ~102, 98, and 86 kD (Fig. 1 *B*), corresponding to the molecular weights of α-, β-, and γ-catenin (plakoglobin), respectively. The stoichiometry of the EcadGFP/catenin complex was similar to that of the endogenous E-cadherin/catenin complex (see Fig. 1, *A* and *B*).

Expression of EcadGFP in HEK 293 EBNA cells that do not normally express cadherin resulted in the formation of condensed cell colonies in the presence of extracellular Ca^{2+} (Fig. 1 *C*), but cell–cell attachments were not

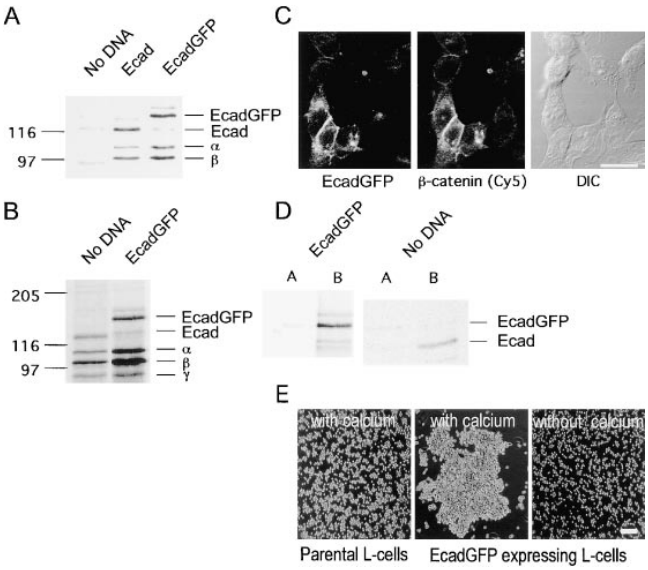

Figure 1. EcadGFP has properties similar to those of endogenous E-cadherin. (*A* and *B*) Catenins were coimmunoprecipitated with EcadGFP from HEK 293 cells transiently transfected with EcadGFP (*A*) or stably transfected MDCK cells (*B*). Cells were labeled with [^{35}S]Met/Cys for 24 h before immunoprecipitation. (*A*) Proteins in cadherin immunoprecipitates are compared among mock-transfected HEK 293 cells (*No DNA*), HEK 293 cells transfected with canine E-cadherin (*Ecad*), and HEK 293 cells transfected with EcadGFP, and (*B*) between untransfected MDCK cells (*No DNA*) and MDCK cells stably transfected with EcadGFP. (*C*) EcadGFP fluorescence and β-catenin immunofluorescence from HEK 293 cells transiently transfected with EcadGFP. Bar, 30 μm. (*D*) Preferential delivery of newly synthesized EcadGFP to the basal-lateral plasma membrane of fully polarized MDCK cells stably transfected with EcadGFP, or of endogenous E-cadherin in untransfected cells (*No DNA*); A, apical membrane; B, basal-lateral membrane. (*E*) Phase contrast images of L-cells and L-cells expressing EcadGFP after 18 h of aggregation in suspension culture in the presence or absence of extracellular Ca^{2+}. Bar, 60 μm.

formed in the absence of extracellular Ca^{2+} (data not shown), demonstrating that the adhesion was mediated by EcadGFP. In HEK 293 EBNA cells, EcadGFP and β-catenin accumulated at the lateral membrane of cell–cell contacts (Fig. 1 *C*), similar to the distributions of endogenous E-cadherin and β-catenin in MDCK cells (Näthke et al., 1994). In addition, newly synthesized EcadGFP was directly targeted to the basal-lateral membrane of polarized MDCK cells, similar to endogenous E-cadherin (Fig. 1 *D*). Also, expression of EcadGFP in mouse L-cells, which do not normally express cadherin, resulted in the formation of large cell aggregates in suspension culture in the presence of extracellular Ca^{2+}, but not in the absence of extracellular Ca^{2+} (Fig. 1 *E*). Finally, the kinetics of aggregation in suspension were identical for wild-type MDCK cells ($t_{1/2}$ = 15.3±2.1 min; n = 2) and MDCK cells expressing EcadGFP ($t_{1/2}$ = 15.9±3.0 min; n = 2), and faster for cells overexpressing EcadGFP. The properties of EcadGFP are indistinguishable from those of endogenous E-cadherin. Thus, EcadGFP can substitute for endogenous E-cadherin in cell–cell adhesion.

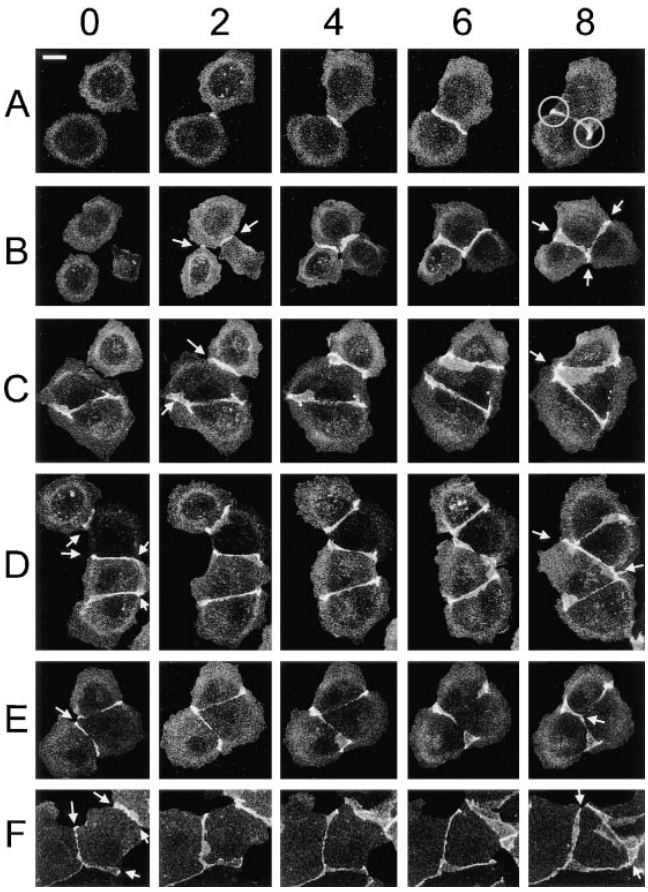

Figure 2. Distribution of EcadGFP during monolayer formation. A single confocal image was collected from EcadGFP expressing cells every 10 min for 12 h at 0.12 μm/pixel at 12 sites. Five representative images from each time-lapse are shown. Elapsed time is indicated on top of each column in h (*0*, *2*, *4*, *6*, and *8*, respectively). The circles in *A* highlight the edges of a cell–cell contact that have developed large aggregates of EcadGFP plaques. The arrows in *B–F*, columns 0 or 2 h point to the well-separated plaques at the edges of developing cell–cell contacts that reorganize into a multicellular vertex by 8 h. Note that the 0-h designation is arbitrarily set as the first time point shown. Bar, 15 μm.

EcadGFP Distribution Changes During Cell–Cell Adhesion

EcadGFP expressing MDCK cells were imaged for 10 h to observe the dynamics of the localization of EcadGFP during formation of contacts between single cells, and during formation of small multicell colonies (Fig. 2). Expression of EcadGFP in single cells was relatively uniform over the plasma membrane with some increased intensity in a circumferential ring at the cell periphery (Fig. 2, *A* and *B*, 0 h). During the formation of cell–cell contacts between two (Fig. 2 *A*) or three (Fig. 2 *B*) cells, or single cells and larger cell clusters (Fig. 2 *C*), EcadGFP fluorescence became significantly more intense at the cell–cell contact during the first 2 h. After at least 2 h, the largest and brightest regions of EcadGFP fluorescence were at the edges of cell–cell contacts; we call these structures plaques (Fig. 2, *circles*). The fluorescence intensity of EcadGFP plaques was 6–10 times greater than that of EcadGFP in noncontacting membranes, and 2–4 times greater than that of EcadGFP in areas of the membrane in the middle of the contact (Fig. 2, *A–C*; 8 h).

When three or more cells developed cell–cell contacts (Fig. 2, *B–D*), EcadGFP plaques from two noncontacting cells often moved towards each other and eventually coalesced to form a vertex of E-cadherin between multiple cells (Fig. 2, *B–D*; compare 2 and 8 h). After forming such a multicellular vertex, EcadGFP reorganized into the center of the colony (Fig. 2 *E*). As more cells formed contacts, this sequential formation of contacts (puncta and plaques) and coalescence of nonadjacent EcadGFP plaques into vertices caused cells to become engulfed into the developing cell monolayer. These steps resulted in the formation of a circumferential ring of both EcadGFP (Fig. 2 *F*) and actin (data not shown) around each cell, similar to the organization of E-cadherin and actin between cells in monolayers of polarized MDCK cells (Näthke et al., 1994). These results demonstrate that we are able to observe with EcadGFP the complete transition of initial contacts between cells through compaction to the establishment of E-cadherin/actin organizations characteristic of a complete epithelium. In general, transitions between initial cell–cell contact (formation of puncta) to E-cadherin plaque formation, to condensation of plaques into multicell vertices were on the time scale of 2–3 h.

To better understand the evolution of these distinct patterns of E-cadherin, the distribution of EcadGFP during development of cell–cell contacts was examined in multisite time-lapse confocal images taken over the course of 3 h (we initially focused on the formation of puncta and plaques during the first two stages of adhesion see below). The cells were then fixed and stained with phalloidin, (which labeled F-actin) and mAb 3G8 (which recognized the extracellular domain of endogenous E-cadherin and EcadGFP), and were imaged. Fig. 3 shows representative contacts from one time-lapse recording. Column 1 of Fig. 3 *A* shows the formation of a contact between two cells over 71 min. During cell–cell adhesion, EcadGFP fluorescence appeared at cell–cell contacts, and then increased in intensity with time and as the contact lengthened. The distribution of EcadGFP and endogenous E-cadherin were re-

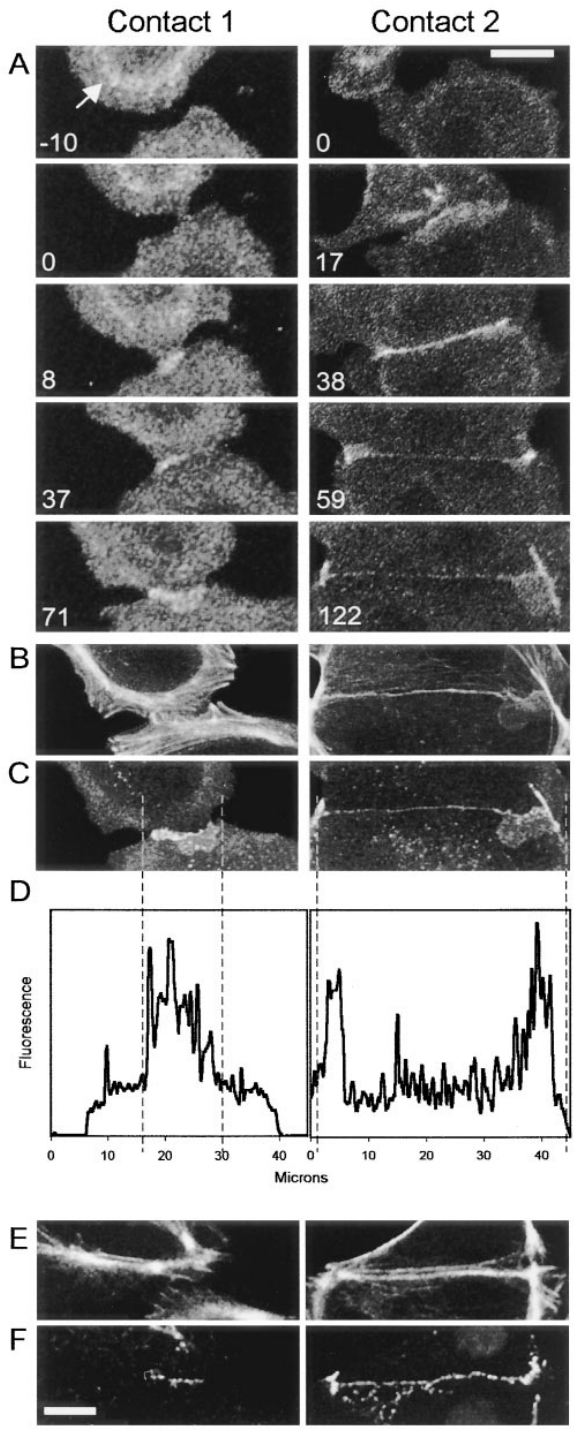

Figure 3. Redistribution of EcadGFP during cell–cell contact occurs in two stages and correlates with reorganization of the actin cytoskeleton. Three 0.3-μm z-sections were collected from EcadGFP-expressing cells every 4.2 min at 0.5 micron/pixel at 6 sites. (*A*) Combined stacks from two sites are shown (*Contact 1* and *Contact 2*). The age of each contact is displayed in min; the zero time point defines when a stable cell–cell contact had formed. Bar, 12 μm. The arrow points to a circumferential pattern of EcadGFP observed in single cells. (*B* and *C*) Immunofluorescence of the same cells stained, after formaldehyde fixation, with rhodamine phalloidin (actin; *B*) and mAb 3G8/CY5 (E-cadherin; *C*). (*D*) EcadGFP organization shown in *C* is plotted as a function of fluorescence intensity (y axis, arbitrary fluorescence units) vs. position in the contact (x axis, μm). The dashed gray lines running between *C* and *D* approximately register the edges of the contact in the image and graph. (*E* and *F*) Triton X-100 extracted wild-type MDCK cells (i.e., without EcadGFP) that had formed a contact for <1 h (*Contact 1*) or >2 h (*Contact 2*) stained with FITC-phalloidin and mAb 3G8/CY5, respectively. Bar, 10 μm.

corded retrospectively with mAb 3G8 (Fig. 3, *1C*), showing that both proteins had coincident distributions as expected (see Fig. 1). Retrospective actin staining (Fig. 3, *1B*) shows that circumferential actin cables were organized parallel to the cell–cell contact interface at this time.

Fig. 3 *A* (*2*) shows similar images of another cell–cell contact that formed over 2 h. At 38 min (Fig. 3, *2A*), EcadGFP was distributed in puncta evenly spaced along the length of the forming contact. However, after 122 min (Fig. 3, *2A*) EcadGFP was prominently localized to plaques at either end of the contact. Retrospective actin staining shows that the most prominent actin cables were also greatly rearranged so that they terminated at each bright plaque of EcadGFP located at the margins of the contact, and were perpendicular to the contact (Fig. 3, *2B*). A much thinner and more discrete line of F-actin staining (Fig. 3, *1B* and *2B*) remained in the orientation parallel to the contact in association with some remaining EcadGFP puncta.

Fig. 3, *E* and *F* shows staining of actin and E-cadherin, respectively, in wild-type MDCK cells (i.e., not expressing EcadGFP) at a contact that is <1 h old (Fig. 3, *1E* and *1F*), and at a contact that is >2 h old (Fig. 3, *2E* and *2F*). The distributions of actin and endogenous E-cadherin in cell–cell contacts are very similar to those of actin and EcadGFP shown in the contacts in Fig. 3, *B* and *C*, respectively, supporting the general conclusion that EcadGFP is fully functional. Furthermore, during cell–cell adhesion, changes in the organization/distribution of EcadGFP are very similar, if not identical, to those of endogenous E-cadherin.

EcadGFP Clusters into Puncta Upon Cell–Cell Contact

Our observation that EcadGFP initially aggregated into puncta during formation of cell–cell contacts is similar to our previous observations in which E-cadherin distributions were determined retrospectively by immunolabeling cells after time-lapse DIC imaging (Adams et al., 1996). However, in that previous study we could not determine the relationship of Triton X-100 insolubility and clustering of E-cadherin, the source of E-cadherin in puncta, the role of the actin cytoskeleton in the spatial organization of puncta, or the dynamics and fate of puncta within the contact. Using EcadGFP, we were able to address these critical problems directly.

The reorganization of EcadGFP during cell–cell adhesion was examined quantitatively by measuring EcadGFP fluorescence intensity over time after initial contact between cells. The graphs in Fig. 3 *D* show quantitative representations of the maximum E-cadherin fluorescence intensity vs. position in the contacts shown in Fig. 3 *C*. The younger contact shows multiple small peaks of fluorescence along the contact, each corresponding to a punctum (Fig. 3, column *1D*). In contrast, the older contact shows two pronounced peaks of fluorescence intensity at the edge of the contact, each corresponding to an EcadGFP plaque (Fig. 3, column *2D*). In addition, there were multi-

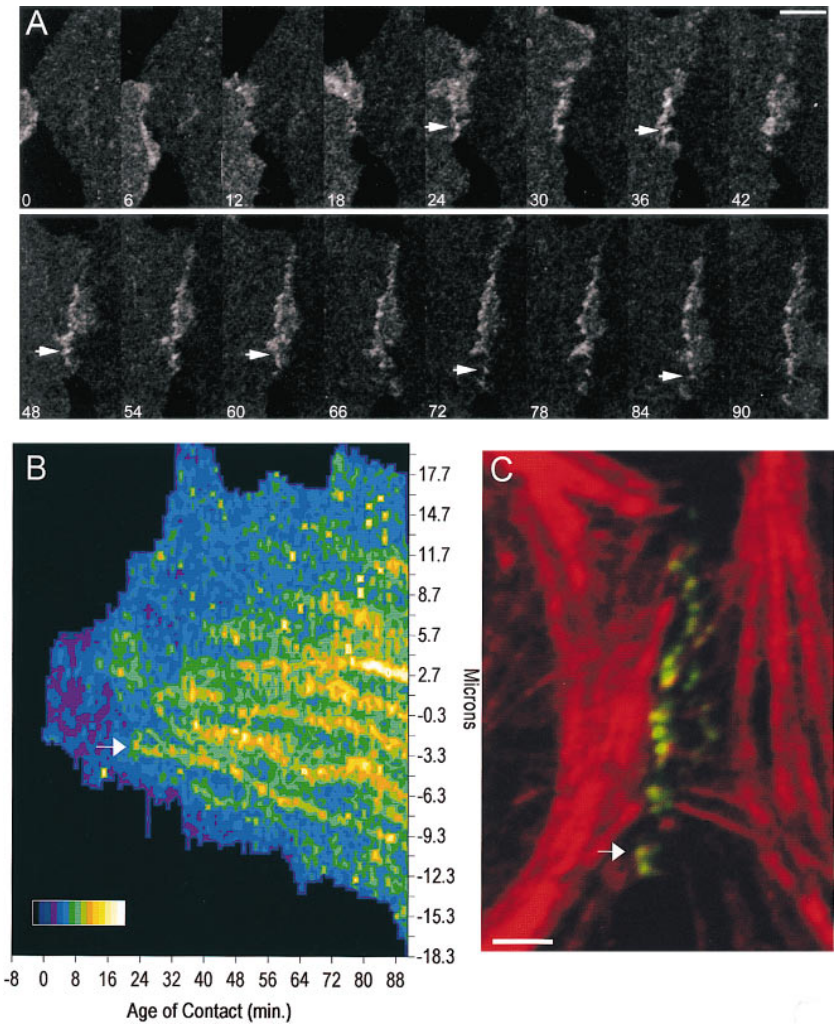

Figure 4. EcadGFP puncta are formed and stabilized along newly formed cell–cell contacts. (*A*) 16 time-lapse images of EcadGFP cells taken from a sequence recorded every 1 min for 100 min at 0.11 μm/pixel; time in min after formation of the contact is shown. Arrows follow a single punctum. (*B*) TIP scan of all of the time-lapse images from the experiment represented in *A*. The contact was divided into 129 0.22-μm sections, and the maximum fluorescence intensity at 100 time points was collected for a total of 12,900 data points. The contact originates at 0 min and 0 μm. Small fluctuations in the apparent intensity of stable puncta are near the limits of instrumental noise sources such as laser output fluctuations and noise processes in the photomultiplier tube detector. (*C*) Double immunofluorescence of the same contact extracted with Triton X-100, fixed with formaldehyde, and stained with rhodamine phalloidin and E-cadherin mAb 3G8/CY5. The arrows in all panels point to the same punctum. Bars: (*A*) 10 μm; (C) 5 μm. (*B*) 0–210 gray scale fluorescence intensity units divided into 15 colors.

ple smaller peaks between the plaques that represented residual puncta within the cell–cell contact.

To gain information about the genesis, lifetime, and position of EcadGFP during initiation of contact formation, a single field of EcadGFP-expressing cells was imaged rapidly at high resolution. Fig. 4 *A* shows representative images from one of these time-lapse recordings. An arrow follows the position of a bright EcadGFP fluorescent punctum at the cell–cell interface. To provide an objective nonbiased format for the quantitative representation of dynamic data like that illustrated in Fig. 4 *A*, we developed the type of representation shown in Fig. 4 *B*. The fluorescence intensity profiles along the length of the contact (e.g., Fig. 3 *D*) were color-coded and combined for each time-lapse frame to provide a color map of EcadGFP intensity distribution along the length of the contact as the contact lengthened. We term such graphs TIP scans. By providing a clear representation of time-dependent changes in EcadGFP fluorescence along the cell–cell contact interface, TIP scans make it relatively easy to discern the organization of EcadGFP during contact formation. Background fluorescence in the TIP scan is contributed by overlapping regions of plasma membrane. Areas of the contact that are brighter than the background cell fluorescence correspond to brighter clusters of EcadGFP. The TIP scan in Fig. 4 *B* shows that the contact in Fig. 4 *A* grew to a length of ~12 μm in ~20 min. The contact then grew more slowly to reach a length of ~35 μm after 90 min.

EcadGFP puncta could be identified in the TIP scan as areas that displayed twice the fluorescence intensity of background. EcadGFP puncta at first appeared close to the initial site of the cell–cell contact, while later they appeared at the margins of the contact (Fig. 4 *B*). We never observed any hint of the insertion of preassembled E-cadherin puncta from the cytoplasm into the membrane at cell–cell contacts, suggesting that E-cadherin puncta originate by de novo aggregation at sites of cell–cell contact, and not from translocation of preassembled aggregates from some other cellular site(s). An arrow in the TIP scan in Fig. 4 *B* also marks the punctum tracked by an arrow in Fig. 4 *A*. The punctum appeared de novo at the contact site and gradually gained intensity over 10 min. By 10–15 min after formation, the intensity level of the punctum remained constant. Such gradual punctum formation was observed in essentially all cases analyzed (see other examples in Fig. 4 *B*), which supports the idea that puncta form in situ from aggregation of molecular subunits.

As the contact lengthened, new EcadGFP puncta appeared sequentially such that the number of puncta remained constant with respect to the length of the contact

(~1 punctum per 1.5 μm contact length; see also Adams et al., 1996). These new puncta also appeared de novo and gradually increased in intensity with time (Fig. 4 *B*). Many of these puncta were spatially stable in the contact interface over time, while some gradually changed position towards the edges of the contact. In general, the fluorescence intensity of puncta was brightest in the oldest part of the contact near the site of initial cell–cell contact (marked as 0 μm), and dimmest at the perimeter of the lengthening.

The EcadGFP puncta evident in these time-lapse sequences were Triton X-100–insoluble. Each EcadGFP punctum observed in the final frames of the time-lapse sequences colocalized with the brightest Triton X-100–insoluble E-cadherin puncta (compare similarly oriented images in Fig. 4 *A*, 90′; and Fig. 4 *C*). EcadGFP puncta were associated with thin cables of actin filaments that emerged from circumferential actin cables oriented parallel to the contact (Fig. 4 *C*). In summary, while we have confirmed our early observation that cell adhesion initiates the formation of E-cadherin puncta, the data presented here demonstrate that a diffuse pool of E-cadherin clusters into puncta in response to cell–cell contact, and that those puncta organize and become stabilized around actin filaments located close to the contacting membranes.

Formation of EcadGFP Plaques at the Contact Margins and Reorganization of the Actin Cytoskeleton

Next, we asked how early E-cadherin puncta are reorganized with actin to further strengthen cell–cell adhesion, and then to cause condensation of cells into multicell colonies. Over longer times (>2 h), EcadGFP and endogenous E-cadherin became organized into large plaques at the margins of the contact (Fig. 2 and Fig. 3, column 2). Fig. 5 *A* shows representative images from a longer time-lapse experiment. After ~1.5 h, two regions of increasing EcadGFP fluorescence appeared and migrated out with the edges of the contact at velocities of up to 0.5 μm/min (Fig. 5). These regions gradually gained up to 10× the average punctum fluorescence intensity over the course of 1 h, in contrast to a punctum that reached maximum fluorescence intensity within 30 min of formation. Approximately 2.5 h after contact nucleation, EcadGFP was heavily concentrated in discrete fluorescent plaques at the margins of the

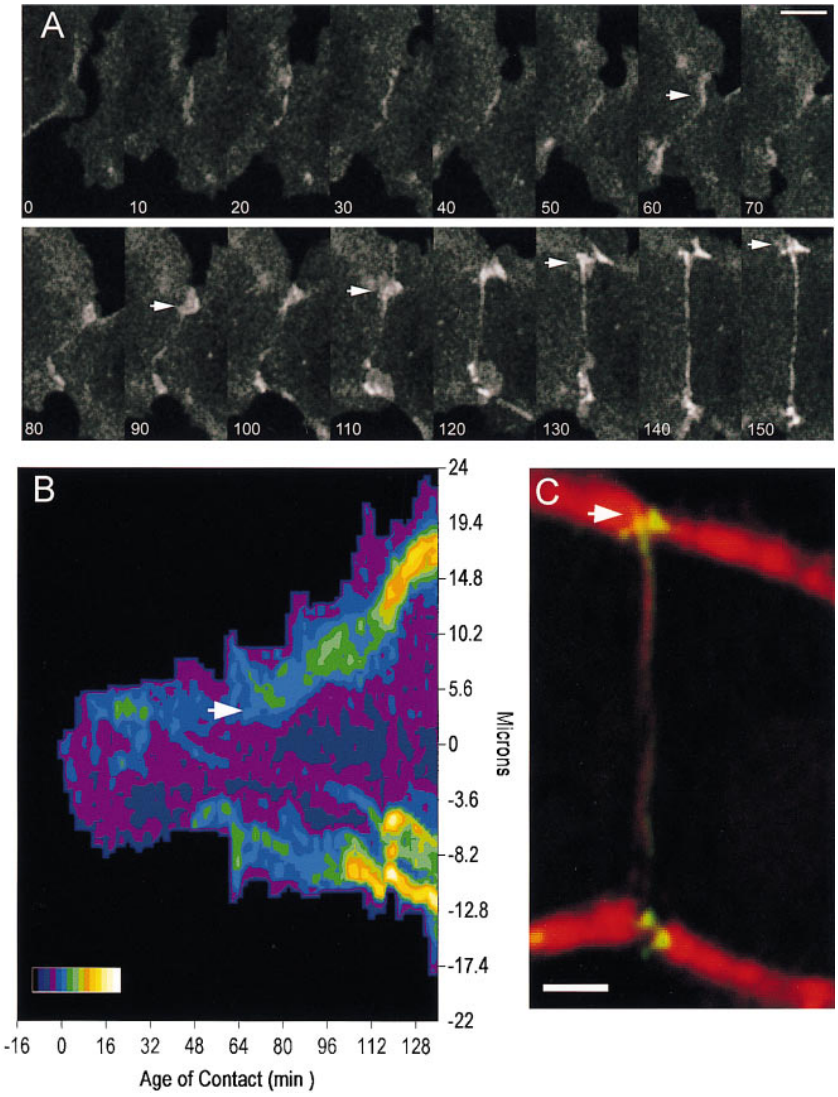

Figure 5. Two large plaques of EcadGFP form and move to the edges of the cell–cell contact. (*A*) 16 time-lapse images of EcadGFP cells taken from a sequence recorded every 2 min for 2.7 h at 0.23 μm/pixel. Arrows follow a single plaque. (*B*) TIP scan of all of the time-lapse images from the experiment represented in *A*. The contact was divided into 101, 0.46-μm sections, and the fluorescence intensity at 85 time points was collected for a total of 8,585 data points. The contact originates at 0 min and 0 μm. Note that the TIP scan at this reduced resolution shows a relatively homogeneous distribution of EcadGFP within the contact during the first hour, whereas the TIP scan at a higher resolution revealed individual punctum (see Fig. 4). (*C*) Double immunofluorescence of the same contact stained with rhodamine phalloidin and E-cadherin mAb 3G8/CY5. The arrows in all panels point to the same plaque. (*B*) 0–151 gray scale fluorescence intensity units divided into 15 colors. Bars: (*A*) 10 μm and (*C*) 5 μm.

contact (Fig. 5, *A* and *B, arrows*). The region of the contact between the two plaques retained a thin line of EcadGFP intensity (compare to Fig. 3, column *2B*). Comparison of the last live EcadGFP images with the retrospective immunofluorescence of E-cadherin and actin (Fig. 5 *C*) shows that EcadGFP plaques were resistant to extraction with Triton X-100, and were sites at which circumferential actin cables terminated.

The gradual increase in the amount of EcadGFP in these plaques might be the result of de novo clustering of EcadGFP around new actin filaments exposed at the margins of the cell–cell contact, or from the aggregation and migration of puncta that had preformed along the length of the contact. To distinguish between these two possibilities, time-lapse images of EcadGFP plaques were recorded rapidly for 300 s at high resolution. Fig. 6 *A* shows a representative montage of images in which a plaque was observed forming from an area of membrane that contained many small puncta (Fig. 6 *A*, *arrowheads*). The small puncta clearly merged together over time to form the larger plaque. The fluorescence intensity of the plaque increased concomitantly with the disappearance of individual puncta. We quantified changes in fluorescence intensity and plotted maximum fluorescence intensity values

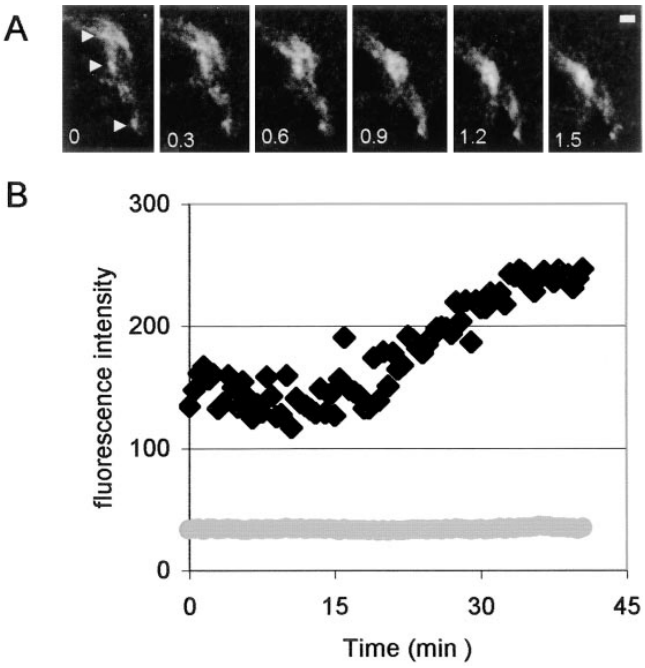

Figure 6. EcadGFP puncta cluster into plaques during transition between early and late stages of adhesion. (*A*) Representative images of a time-lapse sequence taken at 0.8 Hz for 300 s at 0.12 μm/pixel in a region of the cell–cell contact in which a plaque is developing. Time is in min; arrows point to individual puncta; bar, 2 μm. (*B*) Quantitative fluorescence intensities of EcadGFP. The average (*gray circles*) and maximum (*black diamonds*) intensities in a 20-μm^2 region surrounding a developing plaque area are plotted over a 40-min period. The average fluorescence intensity of the same number of EcadGFP in a fixed area is constant regardless of its distribution. However, the maximum fluorescence intensity increases as EcadGFP clusters into a smaller region within that fixed area. For details, see Materials and Methods.

(i.e., the density of EcadGFP) and average fluorescence intensity values (i.e., the total amount of EcadGFP) in large (>10 μm diameter) regions surrounding the edge of the developing contact (Fig. 6 *B*). It is clear that the peak density (Fig. 6 *B*, *black diamonds*), but not the total amount (Fig. 6 *B*, *gray circles*) of EcadGFP increased in the region of the membrane containing the forming plaque. Thus, plaques most likely to arise by lateral clustering of a subset of EcadGFP puncta already formed along the cell–cell contact, and are perhaps supplemented by recruitment of additional EcadGFP molecules in the area of plaque formation.

Circumferential Actin Cables Reorganize During Maturation of Cell–Cell Contacts

To obtain information about the role of actin during the formation and stabilization of cell–cell contacts, cells were treated with the actin-capping agent cytochalasin D (CD). After multisite time-lapse recording for 1 h, EcadGFP cells were treated with 2 μM CD. New cell–cell contacts did not form in the presence of CD (data not shown). Furthermore, young cell–cell contacts (Fig. 7, *A* and *B*) disassembled upon addition of CD (Fig. 7, *C* and *D*). Analogous to an intact monolayer of cells (Hirano et al., 1987), cell–cell contacts within small colonies that were >1 h old did not disassemble during CD treatment. Cells that were in contact for <1 h (Fig. 7 *A*, *upper right* and *lower left*) rounded after CD treatment (compare Fig. 7, *A* and *D*). Greater than 70% of 19 cell–cell contacts that were <1 h old disassembled after treatment with CD (Fig. 7 *G*). In contrast, >15% of 48 contacts that were >1 h old disassembled (Fig. 7 *G*). During CD treatment, EcadGFP formed aggregates that coincided with irregularities in the DIC images (Fig. 7 *D*, *arrow*). These aggregates colocalized with actin and β-catenin (Fig. 7, *E* and *F*) and areas that have been shown to be enriched in the barbed ends of actin filaments (Verkhousky et al., 1997), suggesting that the cadherin/catenin complex may associate with the barbed ends of actin filaments. Furthermore, these data indicate that capping the barbed ends of actin filaments with CD disrupts the ability of E-cadherin puncta, but not plaques to maintain the integrity of cell–cell contacts.

Direct Measurement of EcadGFP Mobility by Photobleach Recovery at Different Stages of Cell–Cell Adhesion

To gain further insight into the assembly dynamics of E-cadherin puncta and plaques, we developed a photobleaching-recovery method to measure the diffusion coefficient, mobile fraction, and redistribution of EcadGFP during different stages of contact development (see Materials and Methods). Photobleaching of cell–cell contacts neither disrupts the organization of adhering plasma membranes, induces retraction of membranes, nor changes membrane movements or dynamics (Fig. 8 *A*). Fig. 8 *A* shows the DIC and EcadGFP images for a live cell before and after photobleaching. After photobleaching, the cells were immediately fixed and stained for E-cadherin and actin. The fluorescence images show that the actin cytoskeleton remained intact, and that the fine spatial organization of E-cadherin at the cell–cell contact was the same as that before pho-

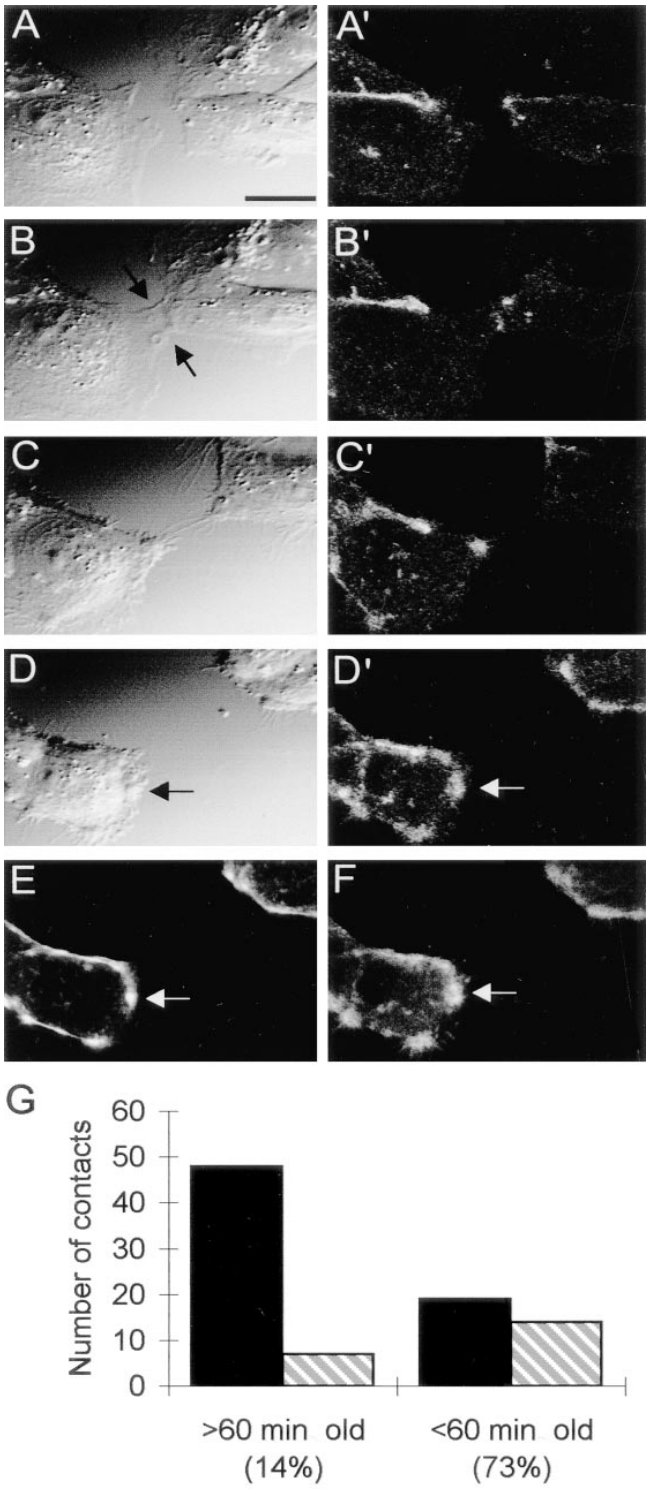

Figure 7. Cytochalasin D selectively disassembles new cell–cell contacts. Representative images of a time-lapse sequence taken at 1 frame/2 min for 2 h at 0.4 μm/pixel before and after adding 2 μM CD. (*A*) 14 min before CD; (*B*) 1 min before CD; (*C*) 30 min after CD; (*D*) 60 min after CD. Immunofluorescence of the same area is shown using rhodamine phalloidin (*E*) or β-catenin/CY5 (*F*). The arrows in *D–F* point to CD-induced EcadGFP clusters; bar, 10 μm. (*G*) The number of cells that were in contact before the time-lapse experiment began (>60 min old), and those that made contact during the imaging experiment (<60 min old) were counted and the totals shown for three independent experiments (*black bars*). The number of those contacts that disassembled within 1 h after CD treatment was determined (*striped bars*). The percentage of cell–cell contacts disassembled by CD treatment is 14% for old contacts and 73% for new contacts.

tobleaching. We also examined whether photobleaching of EcadGFP was reversible. Fig. 8 *B* shows the effects on EcadGFP after 1/2 of a cell was photobleached. The EcadGFP fluorescence was monitored in the photobleached half of the cell (Fig. 8 *B*, *blue*), the nonphotobleached half of the cell (Fig. 8 *B*, *red*), and the entire cell (Fig. 8 *B*, *green*). These data show that the photobleached part of the cell recovered EcadGFP fluorescence while, at the same rate, the nonphotobleached part of the cell lost EcadGFP fluorescence. The average intensity of EcadGFP fluorescence remained constant throughout the entire cell, reflecting the fact that the EcadGFP fluorescence was irreversibly photobleached. These results also show that the entire pool of EcadGFP in the cell was mobile and exchanged within 45 min.

The EcadGFP diffusion coefficient in our system was measured in the thin (1 μm) membrane lamellae between the edge of the cell and circumferential actin cable. To validate our photobleaching methodology, we performed experiments to assess the dependence of fluorescence recovery on the diameter of the photobleached area (Fig. 8 *C*). Table I summarizes data from photobleaching EcadGFP in membrane lamella not involved in cell–cell adhesion using different-sized photobleach areas. These experiments show that EcadGFP diffusion time was related to the square of the photobleach radius as expected from simple diffusion theory; the average value of the diffusion coefficient D was calculated to be $3.6 \pm 1.5 \times 10^{-10}$ cm^2/s. This value is similar to that measured for another transmembrane protein, Na^+, K^+-ATPase, in low-density MDCK cells (Jesaitis and Yguerabide, 1986). We note that previous photobleach-recovery measurements of E-cadherin in the apical membrane of polarized F7p cells yielded a somewhat lower D value of 3.4×10^{-11} cm^2/s (Kusumi et al., 1993), and single particle-tracking measurements of E-cadherin in L-cells yielded a D value of 5.2×10^{-11} cm^2/s (Sako et al., 1998). The difference between these observed diffusion coefficient values of E-cadherin is probably due to differences in methodologies, cell types, and cytoskeletal states.

Our interest here is to compare E-cadherin mobility in different membrane regions during cell–cell adhesion using identical methodologies on the same cell type under carefully controlled conditions. Fig. 8 *D* shows representative EcadGFP images immediately before photobleaching, immediately after photobleaching, and 10 min after recovery in four regions: (*a*) membranes not involved in cell–cell contact; (*b*) new cell–cell contacts; (*c*) puncta; and (*d*) plaques. Note that to measure EcadGFP mobility at cell–cell contacts, we examined the kinetics of recovery of EcadGFP fluorescence after photobleaching in thin lamellae between contacting cells; at those sites, the height of the contact was minimal, EcadGFP fluorescence could be photobleached through the contact, and the subsequent recovery of EcadGFP fluorescence could be tracked with

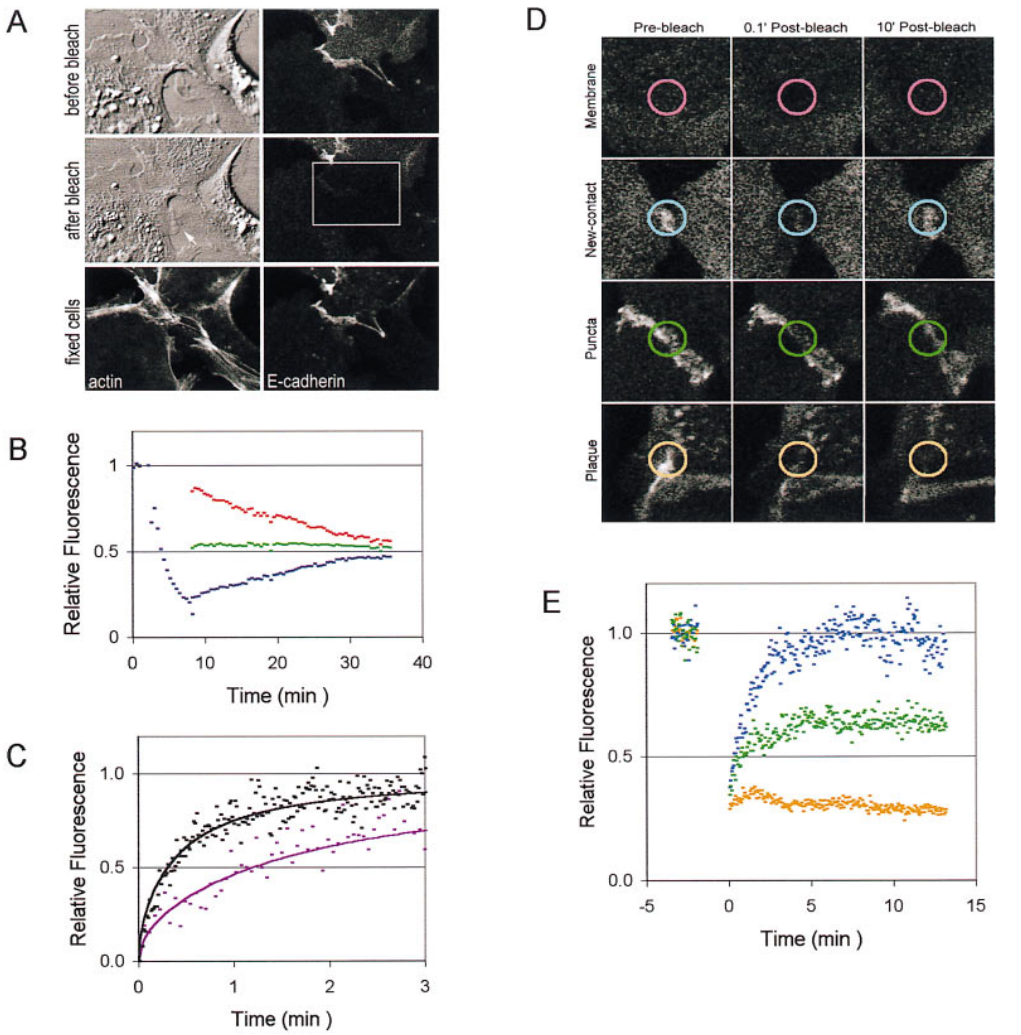

Figure 8. Photobleach-recovery analysis shows a highly mobile pool of EcadGFP coalesces into immobile puncta. *A* shows a live cell before and after photobleaching. The box indicates where the cell was photobleached. The arrow points to an area that formed a contact during the photobleach. The cells were fixed in formaldehyde and stained with phalloidin and mAb 3G8. *B* shows the fluorescence recovery curves of a single noncontacting cell in which half of the cell was photobleached (*blue*). EcadGFP fluorescence of the nonbleached region (*red*) and the entire cell (*green*) was monitored during recovery. Notice that the EcadGFP fluorescence values equalize in the photobleached and nonphotobleached areas. *C* shows the first 3 min of photobleach-recovery data of noncontacting membrane regions photobleached with a 5.8-μm (*pink*) and 3-μm (*black*) circle. The relative fluorescence is scaled between the fluorescence intensity just after bleaching and equilibrium. The lines show the theoretical recovery curves for each region with a diffusion coefficient of 3×10^{-10} cm^2/s. Note that the smaller photobleach circle (*black line*) recovers more quickly. *D* shows images taken before, 0.1 min after, and 10 min after photobleaching a 5.8-μm-diameter circle in a region of membrane not involved in cell–cell contact (*Membrane*), a region of membrane in a <15-min-old contact (*New contact*), a region of membrane in the middle of a <60-min-old contact (*Puncta*), and a membrane at the edge of a >2-h-old contact (*Plaque*). For each experiment, 300 images were collected every 3.2 s at 0.11 μm/pixel. The circles mark the photobleach region, and the colors correspond to the recovery curves shown in *C* (*pink*) and *E*. *E* shows photobleach-recovery data for the bleached contact regions identified in *D*. The relative fluorescence is scaled to the pre-bleach intensity value. The mobile fraction of EcadGFP in the new contact (*blue*), puncta (*green*), and plaque (*orange*) is 100, 50, and <10%, respectively.

high resolution. The recovery curves in Fig. 8 (*C* and *E*) show that EcadGFP in either a contact-free area of the membrane (Fig. 8 *C*) or a newly formed contact (Fig. 8 *E*, *blue*) recovered >90% of fluorescence 15 min after photobleaching. In contrast, EcadGFP in either a punctum or a plaque recovered 50% and <10% fluorescence, respectively. These data indicate that an initially highly mobile pool of EcadGFP becomes increasingly immobilized within developing puncta and plaques.

Fig. 9 shows a TIP scan from an experiment where a 2.8-μm–diameter area was bleached in a 1-h-old contact containing two very bright EcadGFP puncta (Fig. 9, *arrow*). It is clear that bleached puncta partially recovered their fluorescence, concomitant with a partial loss of fluorescence in nonbleached puncta. However, it is also obvious that individual puncta undergo gradual redistributions during these slow recoveries. As the EcadGFP fluorescence recovered, the bleached puncta migrated out of the bleached area, and puncta adjacent to the original bleached area slowly migrated into the bleached area (Fig. 9).

Detailed TIP scan analyses of photobleach recovery data allowed us to make the following generalizations about the dynamics of EcadGFP: (*a*) puncta move as individual units within the cell–cell contact interface during contact expansion; (*b*) puncta on the edge of a fluorescence bleach area recovered their fluorescence first; and (*c*) adjacent nonbleached puncta sometimes exhibited a decrease in fluorescence intensity. These data indicate that the immobilized fraction of EcadGFP is associated with the cytoskeleton, and that cytoskeletal associated EcadGFP moves and exchanges within the cell–cell contact interface.

Table I. E-cadherin/GFP Diffusion Coefficient Measurements

Radius	$D \times 10^{-10}$	SD	*n*
μm	*cm²/s*		
4.1	4.14	1.4	7
2.4	3.6	1.4	10
1.7	3.3	1.7	11
all data	3.6	1.5	26

Data are summarized from photobleaching EcadGFP in membrane lamella not involved in cell–cell adhesion using different-sized photobleach areas. Typically, circular spots of a 120-pixel radius were generated with a 380 × 240 pixel scan raster, and the spot radius (1.7–4.1 μm) at the specimen was varied by adjusting pixel sizes within the range of 0.01–0.05 μm. The photobleaching recovery part of the data was inported into Igor Pro, and the diffusion coefficient (D) was calculated according to the equation $D = 0.224 * r^2/t_{\frac{1}{2}}$, where r is the radius of the bleached region. These experiments show that EcadGFP diffusion time was related to the square of the photobleach radius as expected from simple diffusion theory.

Discussion

E-cadherin plays important roles in cell–cell recognition and adhesion. However, the dynamics of E-cadherin redistribution during the processes of initial cell–cell contact through development of a polarized monolayer are unknown. It is thought that clustering of E-cadherin (Yap et al., 1998) via extracellular homotypic binding (Nose et al., 1988) is sufficient for initial cell–cell interactions: the role of cadherin clusters during the development of older cell colonies is less understood. Furthermore, the dynamic interactions of E-cadherin with intracellular proteins, especially the cytoskeleton, has not been described. By quantitatively analyzing EcadGFP redistribution and mobility in epithelial cells during adhesion development, we provide a new dynamic view of how E-cadherin and the actin cytoskeleton establish strong cell–cell adhesion.

GFP was attached to the COOH terminus of the E-cadherin cytoplasmic domain. The cytoplasmic domain of cadherin binds to catenins, which are required for binding the cadherin/catenin complex to the actin cytoskeleton. Therefore, it was necessary to show that EcadGFP protein has functions identical to those of endogenous E-cadherin. We showed that EcadGFP is fully functional by the following criteria: EcadGFP formed a 1:1:1 stoichiometric complex with α- and β-catenin; EcadGFP precisely colocalized with catenins at cell–cell contacts; EcadGFP was targeted directly from the Golgi to the basal-lateral membrane in polarized MDCK cells; EcadGFP localized to cell–cell contacts and entered a Triton X-100–insoluble pool of proteins only at cell–cell contacts; and EcadGFP induced Ca^{2+}-dependent cell–cell adhesion and condensation in transfected MDCK cells and nonadherent cells (fibroblasts) with kinetics that were qualitatively and quantitatively similar to those of endogenous E-cadherin (Fig. 1). In addition, the kinetics of assembly of EcadGFP puncta in live cells was similar to that measured for the assembly of Triton X-100–insoluble E-cadherin puncta by retrospective immunocytochemistry (Adams et al., 1996), and the formation of cell–cell contacts between MDCK cells expressing EcadGFP and wild-type MDCK cells appeared very similar (compare to Adams et al., 1996). Therefore, the fact that EcadGFP has functions identical to those of endogenous E-cadherin implies that EcadGFP can substitute for endogenous E-cadherin, and that the process of cell–cell adhesion is normal even when levels of endogenous E-cadherin are reduced in the presence of EcadGFP (Fig. 1).

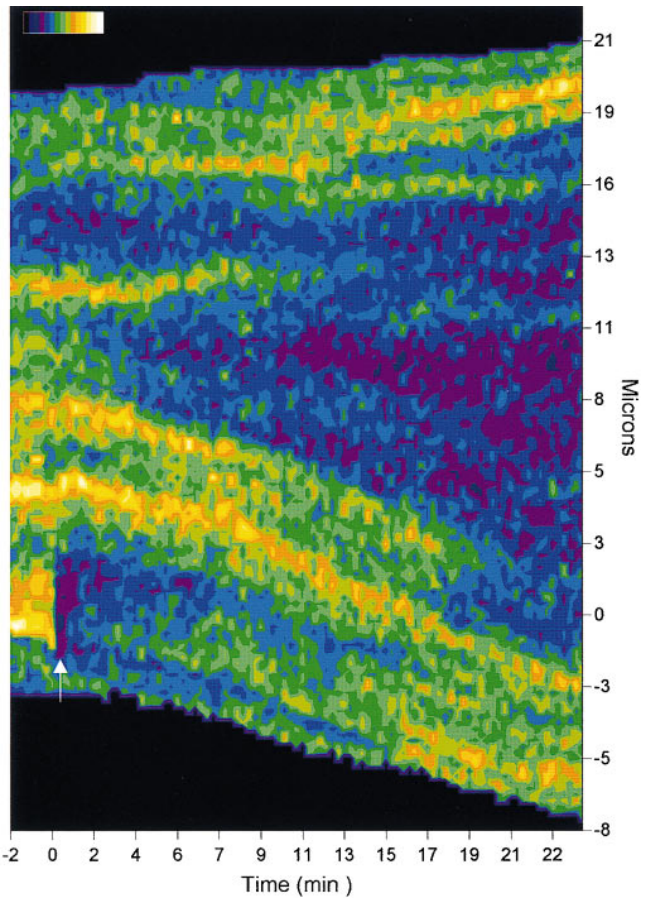

Figure 9. Mobility of E-cadherin puncta within the cell–cell contact interface. Fig. 9 shows a TIP scan of an entire contact during a photobleach-recovery experiment. A newly developing plaque in a 1.5-h-old contact was photobleached with a 2.8-μm-diameter bleach circle (0 mins, 0 μm) on the TIP scan (*arrow*). Images were collected every 16 s for 24 min at 0.11 μm/pixel. The fluorescence intensity scale bar ranges from 0–255 units divided into 15 colors.

We present evidence for three sequential stages of cell–cell adhesion that involve specific changes in E-cadherin and actin cytoskeleton organization. These stages are: (I) clustering of mobile E-cadherin into immobile puncta along the length of the forming contact; (II) reorganization of E-cadherin puncta into plaques at the edges of the contact; and (III) coalescence of E-cadherin plaques to the vertices of contacts among three or more cells.

Stage I

In the first stage of adhesion, E-cadherin spontaneously clusters into puncta at initial sites of developing cell–cell contacts. The formation of E-cadherin puncta results in decreased E-cadherin mobility. In new areas of cell–cell contact (<15 min old), EcadGFP has a high mobile fraction (>90%) and a high diffusion coefficient ($3.6 \pm 1.5 \times 10^{-10}$ cm^2/s). However, where EcadGFP clusters into

puncta and associates with the cytoskeleton, a smaller fraction is mobile (<50% within a 26-μm area). The puncta formed by EcadGFP are very similar in organization and distribution to structures formed by endogenous E-cadherin and catenins that were previously characterized by retrospective immunocytochemistry (Adams et al., 1996; see also Fig. 3).

Weak interactions between extracellular and juxtamembrane domains of cadherins may be sufficient to initiate clustering of the protein in the membrane (Yap et al., 1998). However, interactions between E-cadherin and the actin cytoskeleton are initiated quickly upon cell–cell contact, and these interactions affect the organization of the adhesion complex. We showed that as E-cadherin puncta begin to form during this first stage, they always appear to be associated with the ends of thin actin cables that are oriented toward the contact (Fig. 4). These actin filaments branch from circumferential actin cables that are organized parallel to the forming contact and circumscribe the perimeter of single cells. We speculate that binding actin filaments to E-cadherin/catenin complexes may cause further clustering and stabilization of puncta. This type of cadherin/actin organization has been shown to provide a mechanical linkage between fibroblasts (Ragsdale et al., 1997). Quantitative measurements showed that this initial stage of adhesion coincides with an exponential increase in the strength of adhesion (Angres et al., 1996). Significantly, this strengthening stage was completely inhibited by treatment of cells with CD (Angres et al., 1996; Fig. 7). In the present study we showed that during this initial stage, CD selectively disassembled contacts and caused formation of aggregates that include cell-surface EcadGFP (this study) and probably the barbed ends of actin filaments (Verkhovsky et al., 1997). It is also interesting to note that myosin is involved in the CD-induced aggregation of the barbed ends of actin filaments (Verkhovsky et al., 1997), and that actin treadmilling ceases in areas of developing cell–cell contacts (Gloushankova et al., 1997). We speculate that E-cadherin puncta gradually sequester the barbed ends of actin filaments, and directly or indirectly anchor them to the membrane at cell–cell contacts, resulting in the gradual strengthening of cell–cell adhesion. These changes in actin organization may also set up cytoarchitectural cues for stage II of adhesion.

Stage II

The second stage of contact formation is distinguished by the gradual emergence of much larger E-cadherin clusters that we designate as plaques (Figs. 2, 5, and 6). Generally, one plaque is observed to form at either end of the developing contact where the reorganized circumferential actin cables terminate. Identical plaques were formed by endogenous E-cadherin in compacted MDCK cell–cell contacts (Fig. 3). Using EcadGFP, we showed that these plaques arose by lateral clustering of a subset of puncta that were formed during the first stage of adhesion and the continual immobilization of a mobile pool of EcadGFP (Fig. 9). Plaque formation resulted in a further decrease in the mobile fraction of E-cadherin to <10%. Using TIP scans, we found that during plaque formation, EcadGFP puncta traveled within the cell–cell contact interface to the margins of the contacts at velocities of up to 0.5 μm/min (Fig. 5), which is similar to the velocity of translocation of ConA beads along cell–cell contacts (Gloushankova et al., 1997).

During the second stage of contact formation, circumferential actin cables rearrange from a parallel to a perpendicular orientation with respect to the cell–cell contact (Fig. 5). The reorganization of actin appears to be different in MDCK cells and fibroblasts (Yonemura et al., 1995), which raises the possibility that the strength of the interactions between E-cadherin and actin might be responsible for specific differences in actin dynamics between these two cell types. A consequence of the reorganization of E-cadherin and the actin cytoskeleton is the compaction of contacting cells, which is a clear sign of the establishment of strong cell–cell adhesion and cells maximizing the contacting surfaces between them (Fig. 2). We showed that these compacted cell–cell contacts are resistant to disassembly by CD, indicating either that these contacts have become mechanically resistant to depolymerization of actin, or the barbed ends of the circumferential actin cables are firmly embedded within E-cadherin plaques and are no longer accessible to CD.

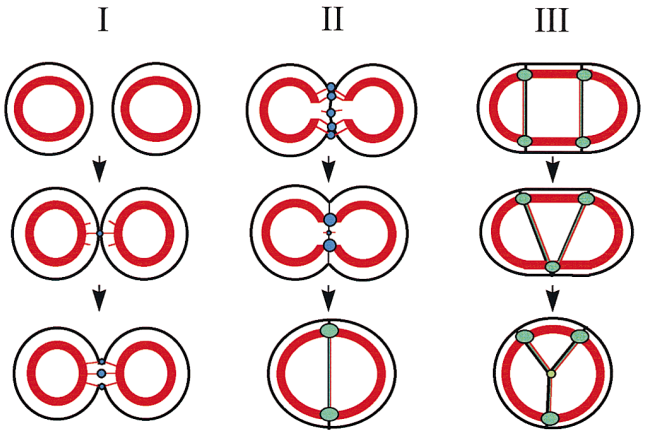

Figure 10. A three-stage model for cell–cell adhesion and colony formation. Stage I: multiple E-cadherin puncta form along the developing contact and loosly hold contacting cells together. A circumferential actin cable (*thick red line*) surrounds isolated cells. As cells adhere, E-cadherin clusters into puncta within the cell–cell contact interface (*blue circle*) and rapidly associates with thin actin bundles and filaments (*thin red lines*). As the contact lengthens, puncta continue to develop along the length of the contact at a constant average density during the first 2 h. Stage II: E-cadherin plaques develop at the edges of the contact which compact and strengthen cell–cell interactions. Stabilization of actin filaments by E-cadherin puncta within the cell–cell contact results in gradual dissolution of the circumferential actin cable behind the developing contact and insertion of the circumferential actin cables into the cell–cell contact accompanied by additional clustering of E-cadherin puncta into E-cadherin plaques (*green ovals*). Between cell plaques, E-cadherin is more diffusely distributed (*green line*) and associates with actin filaments oriented along the axis of the cell–cell contact (*red line*). Stage III: E-cadherin plaques cinch together to form multicellular vertices, further condensing cell colonies. In multicellular colonies, contractility within the circumferential actin cable brings E-cadherin plaques from adjacent cells together. Dynamics within the cytoskeleton result in continual rearrangement.

Stage III

E-cadherin plaque formation coordinates circumferential actin cables to cell–cell contact and maximizes the area of membrane involved in the contact between two cells. When more than two cells form contacts, E-cadherin plaques and actin cables continue to reorganize to form a more compact cell colony (Fig. 2). This process of condensation involves movement of E-cadherin plaques towards each other until they have coalesced to form a vertex among three or more cells (Fig. 2, *C* and *D*). We suggest that E-cadherin plaques are cinched together by contraction of the actin cables that coordinate the plaques within the multicell colony. This reorganization of E-cadherin changed the shape of cells from rather cubiodal after plaque formation to cone-shaped after cell condensation in colonies; the vertices of E-cadherin were located at the tip of the cone (Fig. 2, *B–D*). The formation of cone-shaped cells is redolent of the effects of purse-string contraction of circumferential actin filaments during wound healing in vitro (Bement et al., 1993) and in vivo (Martin and Lewis, 1992; Brock et al., 1996). Previous studies have shown that contraction of cell monolayers around a wound coincides with reorganization of actin cables, myosin II, tropomyosin, and other actin-associated proteins on the membrane adjacent to the wound. It is assumed that actin–myosin contraction pulls on membranes at the edge of the wound to close the opening between cells. We suggest that circumferential actin contraction initiated during cell–cell compaction continues until an equilibrium, perhaps equal tension, is reached between the circumferential actin bundles throughout the forming multicell colony. Studies are underway to test the roles of actin and actin contractility in this stage of adhesion and cell reorganization.

A Model

In summary, we suggest a model for how contacts between cells are initiated, strengthened, compacted, and condensed as cells transform from the migratory phenotype of a single cell to a sedentary phenotype of one cell in a multicell monolayer. Cell–cell adhesion is initiated by weak binding between extracellular domains of E-cadherin that are present in a highly mobile pool at the plasma membrane. At or near the same time, E-cadherin/catenin complexes attach to actin filaments that branch from actin cables that circumscribe the perimeter of migratory cells. These two processes act synergistically to assemble puncta, which, as a group, are sufficiently adhesive to hold the nascent cell–cell contact together (Fig. 10, stage I). Subsequently, there is a change in actin dynamics as actin treadmilling ceases in areas of cell–cell contact, perhaps due to sequestration of the barbed ends of actin filaments into E-cadherin puncta. We hypothesize that reduced actin treadmilling causes the dissolution of the circumferential actin cables immediately adjacent to the developing contact. It is also possible that a signaling event at the cell surface induced by cell–cell adhesion causes a change in the organization or polymerized state of the circumferential actin cables adjacent to the contact site. We suggest that stabilization of actin via the clustered cadherin/catenin complex engages the myosin II clutch (Suter et al., 1998), thereby inducing translocation of circumferential actin cables and the rest of the cell body to the cell–cell contact interface and the rapid movement of associated E-cadherin puncta into large plaques. This coordinated reorganization of E-cadherin and the actin cytoskeleton results in the establishment of strong compacted cell–cell contacts and the generation of an actin cable that circumscribes the free edges of the newly contacting cells and is embedded into either side of a E-cadherin plaque at the margins of the contact (Fig. 10, stage II).

The third stage of adhesion (Fig. 10, stage III) is initiated once another cell joins a two-cell colony. Additional cells join larger cell colonies using the same mechanisms outlined in stages I and II. When three cells contact, two cell–cell contacts and two free edges flank a center cell. Two perimeter actin cables are localized to the free edges of the center cell, and are further linked at E-cadherin plaques to the circumferential actin cables from the two flanking cells. This organization is unstable, and results in further reorganization of E-cadherin puncta, and the circumferential actin cytoskeleton. This reorganization is initiated by the lateral translocation of the E-cadherin plaques on one side of the colony towards each other until they coalesce. This triangular organization of E-cadherin undergoes a final rearrangement as the cells condense and maximize contacts between each other (Fig. 10, stage III). In stage III, we suggest that one of the perimeter actin cables of the center cell dominates, exerts tension on the E-cadherin plaques, and slowly pulls the plaques from the outside cells together. The colony continues to reorganize into a stable configuration of a circle, with each cell connected together on one side sharing a common vertex in the middle of the colony.

Additional cells systematically join a multicellular colony as described above. E-cadherin and actin in newly forming cell–cell contacts reorganize, and then cinch together adjacent plaques attached to actin cables at the free cell edges (Fig. 2, *D* and *E*). Eventually some cells will become engulfed by a multicellular colony such that there is no longer a circumferential actin cable, and the cell is surrounded by contacts on all sides. There still exist larger clusters of E-cadherin at the vertices of cells within the multicellular colony, and the cells are probably still able to exert tension on each other through these regions to maximize the contact area. The organization of actin in the multicellular colony is now distinctly different from that in a cell–cell contact that is <1 h old, and is characterized by thin actin bundles running parallel to the cell–cell contact in association with E-cadherin (see Fig. 3). These E-cadherin and actin organizations are also characteristic of the mature monolayer.

Our findings reveal a very tight coordination among cadherin binding, aggregation, adhesion events, and dramatic reorganizations of the actin cytoskeleton. These reorganizations occur in parallel with transitions from weak initial adhesion to strong adhesions associated with cell–cell compactions, condensations of cells into colonies, and formation of a belt of cadherin and actin as observed in mature monolayers. These results provide a new framework for future studies aimed at identifying the effects of other regulatory molecules (e.g., GTPases, kinases, and cytoskeletal motors) and cadherin-associated proteins (e.g.,

p120^{CAS}) on these distinct adhesive stages of cell–cell adhesion.

We thank members of the Nelson and Smith labs and Chris Hazuka for their comments during the course of this work, Dr. Richard Lewis for help programming diffusion solutions in Igor Pro, Dr. Lee Rubin (University College London) for the canine E-cadherin cDNA clone, and Dr. Brian Seed (Harvard Medical School) for the generous gift of humanized codon-preference-adjusted red-shifted GFP before its publication. We also thank Dr. David Loftus for his help with the aggregation assay.

W.J. Nelson and S.J Smith were supported by grants from the National Institutes of Health and The Mathers Charitable Foundation. Y.-T. Chen is a recipient of a postdoctoral fellowship award from National Kidney Foundation.

Received for publication 13 February 1998 and in revised form 1 June 1998.

References

Aberle, H., S. Butz, J. Stappert, H. Weissig, R. Kemler, and H. Hoschuetzky. 1994. Assembly of the cadherin-catenin complex in vitro with recombinant proteins. *J. Cell Sci.* 107:3655–3663.

Aberle, H., H. Schwartz, and R. Kemler. 1996. Cadherin-catenin complex: protein interactions and their implications for cadherin function. *J. Cell. Biochem.* 61:514–523.

Adams, C.L., W.J. Nelson, and S.J. Smith. 1996. Quantitative analysis of cadherin-catenin-actin reorganization during development of cell-cell adhesion. *J. Cell Biol.* 135:1899–1911.

Angres, B., A. Barth, and W.J. Nelson. 1996. Mechanisms for transition from initial to stable cell-cell adhesion: kinetic analysis of E-cadherin-mediated adhesion using a quantitative adhesion assay. *J. Cell Biol.* 134:549–557.

Axelrod, D., D.E. Koppel, J. Schlessinger, E. Elson, and W.W. Webb. 1976. Mobility measurement by analysis of fluorescence photobleaching recovery kinetics. *Biophys. J.* 16:1055–1069.

Bement, W.M., P. Forscher, and M.S. Mooseker. 1993. A novel cytoskeletal structure involved in purse string wound closure and cell polarity maintenance. *J. Cell Biol.* 121:565–578.

Brieher, W.M., A.S. Yap, and B.M. Gumbiner. 1996. Lateral dimerization is required for the homophilic binding activity of C-cadherin. *J. Cell Biol.* 135: 487–496.

Brock, J., K. Midwinter, J. Lewis, and P. Martin. 1996. Healing of incisional wounds in the embryonic chick wing bud: characterization of the actin purse-string and demonstration of a requirement for Rho activation. *J Cell Biol.* 135:1097–1107.

Chen, Y.-T., C. Holcomb, and H.-P. Moore. 1993. Expression and localization of two low molecular weight GTP-binding proteins, Rab8 and Rab10, by epitope tag. *Proc. Natl. Acad. Sci. USA.* 90:6508–6512.

Cooper, M.W., and S.J. Smith. 1992. A real-time analysis of growth cone-target cell interactions during the formation of stable contacts between hippocampal neurons in culture. *J. Neurobiol.* 23:814–828.

Fannon, A.M., and D.R. Colman. 1996. A model for central synaptic junctional complex formation based on the differential adhesive specificities of the cadherins. *Neuron.* 17:423–434.

Gloushankova, N.A., N.A. Alieva, M.F. Krendel, E.M. Bonder, H.H. Feder, J.M. Vasiliev, and I.M. Gelfand. 1997. Cell-cell contact changes the dynamics of lamellar activity in nontransformed epitheliocytes but not in their ras-transformed descendants. *Proc. Natl. Acad. Sci. USA.* 94:879–883.

Graeve, L., A. Patzak, K. Drickamer, and E. Rodriguez-Boulan. 1990. Polarized expression of functional rat liver asialoglycoprotein receptor in transfected Madin-Darby canine kidney cells. *J. Biol. Chem.* 265:1216–1224.

Haas, J., E.C. Park, and B. Seed. 1996. Codon usage limitation in the expression of HIV-1 envelope glycoprotein. *Curr. Biol.* 6:315–324.

Herrenknecht, K., M. Ozawa, C. Eckerskorn, F. Lottspeich, M. Lenter, and R. Kemler. 1991. The uvomorulin-anchorage protein α-catenin is a vinculin homologue. *Proc. Natl. Acad. Sci. USA.* 88:9156–9160.

Hirano, S., A. Nose, K. Hatta, A. Kawakami, and M. Takeichi. 1987. Calcium-dependent cell-cell adhesion molecules (cadherins): Subclass specificities and possible involvement of actin bundles. *J. Cell Biol.* 105:2501–2510.

Jesaitis, A.J., and J. Yguerabide. 1986. The lateral mobility of the (Na^+,K^+)-dependent ATPase in Madin-Darby canine kidney cells. *J. Cell Biol.* 102: 1256–1263.

Jou, T.-S., D. Stewart, J. Stappert, W. Nelson, and J. Marrs. 1995. Genetic and biochemical dissection of protein linkages in the cadherin-catenin complex. *Proc. Natl. Acad. Sci. USA.* 92:5067–5071.

Kinsella, T.M., and G.P. Nolan. 1996. Episomal vectors rapidly and stably produce high-titer recombinant retrovirus. *Hum. Gene Ther.* 7:1405–1413.

Knudsen, K.A., A.P. Soler, K.R. Johnson, and M.J. Wheelock. 1995. Interaction of α-actinin with the cadherin/catenin cell-cell adhesion complex via α-catenin. *J. Cell Biol.* 130:67–77.

Kusumi, A., Y. Sako, and M. Yamamoto. 1993. Confined lateral diffusion of membrane receptors as studied by single particle tracking (nanovid microscopy). Effects of calcium-induced differentiation in cultured epithelial cells. *Biophys. J.* 65:2021–2040.

Livingstone, M.S. 1988. Art, illusion and the visual system. *Sci. Am.* 258:78–85.

Martin, P., and J. Lewis. 1992. Actin cables and epidermal movement in embryonic wound healing. *Nature.* 360:179–183.

McNeill, H., T.A. Ryan, S.J. Smith, and W.J. Nelson. 1993. Spatial and temporal dissection of immediate and early events following cadherin-mediated epithelial cell adhesion. *J. Cell Biol.* 120:1217–1226.

Martinek, S., and U. Gaul. 1997. Neural development: how cadherins zipper up neural circuits. *Curr. Biol.* 7:R712–R715.

Nagafuchi, A., and M. Takeichi. 1988. Cell binding function of E-cadherin is regulated by the cytoplasmic domain. *EMBO (Eur. Mol. Biol. Organ.) J.* 7:3679–3684.

Nagar, B., M. Overduin, M. Ikura, and J.M. Rini. 1996. Structural basis of calcium-induced E-cadherin rigidification and dimerization. *Nature.* 380:360–364.

Näthke, I.S., L. Hinck, J.R. Swedlow, J. Papkoff, and W.J. Nelson. 1994. Defining interactions and distributions of cadherin and catenin complexes in polarized epithelial cells. *J. Cell Biol.* 125:1341–1352.

Nose, A., A. Nagafuchi, and M. Takeichi. 1988. Expressed recombinant cadherins mediate cell sorting in model systems. *Cell.* 54:993–1001.

Ozawa, M., H. Baribault, and R. Kemler. 1989. The cytoplasmic domain of the cell adhesion molecule uvomorulin associates with three independent proteins structurally related in different species. *EMBO (Eur. Mol. Biol. Organ.) J.* 8:1711–1717.

Ozawa, M., and R. Kemler. 1992. Molecular organization of the uvomorulin-catenin complex. *J. Cell Biol.* 116:989–996.

Ragsdale, K.G., J. Phelps, and K. Luby-Phelps. 1997. Viscoelastic response of fibroblasts to tension transmitted through adherens junctions. *Biophys. J.* 73: 2798–2808.

Reynolds, A.B., J. Daniel, P.D. McCrea, M.J. Wheelock, J. Wu, and Z. Zhang. 1994. Identification of a new catenin: The tyrosine kinase substrate p120^{cas} associates with E-cadherin complexes. *Mol. Cell. Biol.* 14:8333–8342.

Rimm, D.L., E.R. Koslov, P. Kebriaei, C.D. Cianci, and J.S. Morrow. 1995. α1(E)-catenin is an actin-binding and -bundling protein mediating the attachment of F-actin to the membrane adhesion complex. *Proc. Natl. Acad. Sci. USA.* 92:8813–8817.

Sako, Y., A. Nagafuchi, S. Tsukita, M. Takeichi, and A. Kusumi. 1998. Cytoplasmic regulation of the movement of E-cadherin on the free cell surface as studied by optical tweezers and single particle tracking: corralling and tethering by the membrane skeleton. *J. Cell Biol.* 140:1227–1240.

Shapiro, L., A.M. Fannon, P.D. Kwong, A. Thompson, M.S. Lehmann, G. Grubel, J.-F. Legrand, J. Als-Nielsen, D.R. Colman, and W.A. Hendrickson. 1995. Structural basis of cell-cell adhesion by cadherins. *Nature.* 372:327–337.

Small, V.J., K. Anderson, and K. Rottner. 1996. Actin and the coordination of protrusion, attachment and retraction in cell crawling. *Biosci. Rep.* 16:351–368.

Soumpasis, D.M. 1983. Theoretical analysis of fluorescence photobleaching recovery experiments. *Biophys. J.* 41:95–97.

Southern, P.J., and P. Berg. 1982. Transformation of mammalian cells to antibiotic resistance with a bacterial gene under control of the SV40 early region promoter. *J. Mol. Appl. Genet.* 1:327–341.

Suter, D.M., L.D. Errante, V. Belotserkovsky, and P. Forscher. 1998. The Ig superfamily cell adhesion molecule, apCAM, mediates growth cone steering by substrate-cytoskeletal coupling. *J. Cell Biol.* 141:227–240.

Steinberg, M.S., and M. Takeichi. 1994. Experimental specification of cell sorting, tissue spreading, and specific spatial patterning by quantitative differences in cadherin expression. *Proc. Natl. Acad. Sci. USA.* 91:206–209.

Steinberg, M.S. 1996. Adhesion in development: an historical overview. *Dev. Biol.* 180:377–388.

Takeichi, M. 1991. Cadherin cell adhesion receptors as a morphogenetic regulator. *Science.* 251:1451–1455.

Takeichi, M. 1987. Cadherins: a molecular family essential for selective cell-cell adhesion and animal morphogenesis. *Trends Genet.* 3:213–217.

Townes, P.L., and J. Holtfreter. 1955. Directed movement and selective adhesion of embryonic amphibian cells. *J. Exp. Zool.* 128:53–120.

Uchida, N., Y. Honjo, K.R. Johnson, M.J. Wheelock, and M. Takeichi. 1996. The catenin/cadherin adhesion system is localized in synaptic junctions bordering transmitter release zones. *J. Cell Biol.* 135:767–779.

Verkhovsky, A.B., T.M. Svitkina, and G.G. Borisy. 1997. Polarity sorting of actin filaments in cytochalasin-treated fibroblasts. *J. Cell Sci.* 110:1693–1704.

Wollner, D.A., K.A. Krzeminski, and W.J. Nelson. 1992. Remodeling the cell surface distribution of membrane proteins during the development of epithelial cell polarity. *J. Cell Biol.* 116:889–899.

Yap, A.S., W.M. Brieher, M. Pruschy, and B.M. Gumbiner. 1997. Lateral clustering of the adhesive ectodomain: a fundamental determinant of cadherin function. *Curr. Biol.* 7:308–315.

Yap, A.S., C.M. Niessen, and B.M. Gumbiner. 1998. The juxtamembrane region of the cadherin cytoplasmic tail supports lateral clustering, adhesive strengthening, and interaction with p120^{ctn}. *J. Cell Biol.* 141:779–789.

Yonemura, S., M. Itoh, A. Nagafuchi, and S. Tsukita. 1995. Cell-to-cell adherens junction formation and actin filament organization: similarities and differences between non-polarized fibroblasts and polarized epithelial cells. *J. Cell Sci.* 108:127–142.